scientific reports

Check for updates

OPEN

Rhodiola crenulata induces apoptosis in bone metastatic breast cancer cells via activation of caspase-9 and downregulation of MtMP activity

Preetham Ravi[1], Haneesh Jasuja[1], Dipayan Sarkar[2], Benjamin Vahidi Pashaki[1], Hanmant K. Gaikwad[1], Pooyan Vahidi Pashaki[1], Dinesh R. Katti[1], Kalidas Shetty[3] & Kalpana S. Katti[1]✉

Breast cancer cells have the propensity to metastasize to bone, resulting in altered growth, chemoresistance, and causing skeletal failures, often leading to death in patients. There is a scarcity of effective therapeutics for bone metastasized breast cancer due to the lack of accurate drug screening metastasis models. We utilize a unique 3D in vitro nano clay-based scaffold model as a testbed for bone metastatic breast cancer for drug screening applications. *Rhodiola crenulata*, a Tibetan plant-based extract, has been previously explored for primary-site breast cancer. However, its effect on bone metastasized breast cancer cells is unknown. In the present study, we evaluated the cytotoxicity of *R. crenulata* extract on bone metastatic breast cancer using testbeds and compared the results with 2D cultured cells. We observed that *R. crenulata* induced apoptosis in bone metastasized breast cancer cells grown on a 3D in vitro testbed by upregulating pro-apoptotic proteins, p53, and caspase-9. Alternatively, we observed that bone cells remain unaffected by the treatment of *R. crenulata*. For the first time, we demonstrated the anticancer capabilities of *R. crenulat*a against bone metastasis of breast cancer. *R. crenulata* is a robust therapeutic candidate for bone metastasis, shown to induce death in bone metastatic breast cancer while unaffecting healthy bone.

Keywords Breast cancer, Bone metastasis, 3D testbeds, *Rhodiola crenulata*, Apoptosis, Anticancer therapy

Abbreviations

Bax	Bcl-2-associated X protein
Bak	Bcl-2 homologous antagonist/killer
Bcl-2	B-cell lymphoma 2
DAPI	4′,6-Diamidino-2-phenylindole
DMEM	Dulbecco's modified eagle medium
E.R.	Estrogen receptor
EMEM	Eagle's minimal essential medium
FBS	Fetal bovine serum
HAP	Hydroxyapatite
HER2	Human epidermal growth factor receptor 2
hMSCs	Human mesenchymal stem cells
IC-50	Half-maximal inhibitory concentration
MCF-7	Michigan Cancer Foundation-7
MDA-MB-231/MM 231	Monroe Dunaway Anderson-Mammary Luminal B-231
p53	Tumor suppressor protein p53
PCL	Polycaprolactone

[1]Department of Civil, Construction and Environmental Engineering, North Dakota State University, 1410 14th Ave N, Fargo, ND 58105, USA. [2]United States Department of Agriculture, Fargo, ND 58105, USA. [3]Department of Plant Sciences, North Dakota State University, Fargo, ND 58105, USA. ✉email: Kalpana.Katti@ndsu.edu

ROS	Reactive oxygen species
FITC	Fluorescein isothiocyanate
PBS	Phosphate buffered saline
Caspase	Cysteine-aspartic acid protease

According to the National Cancer Institute, cancer is one of the leading causes of death worldwide. New cancer cases are predicted to rise to over 23 million by 2030. The WHO reports 2.26 M cases of breast cancer each year and 684,996 deaths. Nearly 12.4% of all women in the United States will be diagnosed with breast cancer during their lifetime. Roughly 287,000 cases of breast cancer were diagnosed in 2022 among women[1]. In 2022, over 43,000 breast cancer-related deaths were reported. The majority of the deaths occur due to metastasis of breast cancer. Nearly 6% of breast cancer tends to metastasize to secondary organs, such as bone, lungs, liver, and brain. Breast cancer metastasizes to the bone, resulting in the death of 70% of the patients within five years due to various bone-related complications such as hypercalcemia, bone fractures, cancer cachexia, and spinal cord compression[1,2]. Currently, chemotherapy and invasive surgery are the primary therapeutic options. Aromatase inhibitors and drugs like Trastuzumab have also been used to reduce tumor formation in breast cancer patients that are hormone-receptor-positive or HER2-positive, respectively[1]. However, due to the lack of curative treatment for advanced-stage breast cancer, there is a need for new therapeutics that should be more effective and possess fewer side effects. Recently, plant-based therapeutics, such as phytochemically-enriched plant extracts, have shown strong anticancer effects[3,4] and are proving to be viable chemo-preventative alternatives due to their ability to scavenge free radicals and neutralize free radical-cytotoxicity.

In cancer cells, inefficient oxidative phosphorylation leads to the uncontrollable formation of free radicals or ROS production[5,6]. Cancer cells promote the functioning of anti-apoptotic factors such as Bcl-2 and p53 that lead to chemoresistance[7]. Biomarker p53 is related to the development/progression of cancer by regulating the cell cycle when cancer suppression-associated DNA is damaged. The dysregulation of p53 can be linked to chemoresistance in cancer. Alternatively, the Bcl-2 protein is a part of the anti-apoptotic family linked to chemoresistance. This family of proteins can be found to be upregulated in chemo-resistant cancer[8]. The inhibition of Bcl-2 and activation of Bax and Bak lead to tumor apoptosis[9]. Additionally, the activation of caspase proteins is responsible for executing apoptosis[10].

Rhodiola crenulata (*R. crenulata*) is a plant species commonly used in traditional oriental medicine. Plant extracts of the Rhodiola species are rich sources of phenolic antioxidants and have exhibited anti-inflammatory properties[11–13]. Rhodiola species, also known as the "golden root," is a medicinal herb grown in northern Asia, the cold regions of Europe, and North America[14]. Extracts from the Rhodiola species are characterized as "adaptogens," which is a term referencing the compound's innate ability to maintain physiological well-being while being exposed to stress[15,16]. Rhodiola extracts can prevent mutagen-DNA reactions, resulting in cellular repair mechanisms. A recent study reports its anti-proliferative properties against multiple cancer types: B16-B10 melanoma, NB-1691 neuroblastoma, MDA-MB-231, V14-tumors in mice, and MCF-7 cell lines[15,17–21]. Specifically, effects were observed in both in vitro and in vivo conditions[22–25]. Previous studies report the effectiveness of *R. crenulata* on breast cancer cells grown in 2D in vitro cultures, in vivo cultures, and tumorsphere culture assays. However, their efficacy in treating bone metastatic cancer has yet to be investigated.

The development of effective therapeutics for late-stage breast cancer metastasis to bone is dependent on the understanding of metastatic transition. Researchers have previously utilized two-dimensional (2D) monolayer systems to study signaling pathways and cellular responses to traditional therapeutics. However, the 2D monolayer fails to recapitulate the 3D microenvironment of human biology. Cell–matrix and cell–cell interactions govern cell behavior in a three-dimensional (3D) environment, including cancer cells[26]. Traditionally, 3D environments have been simulated through animal models. Human cancer cells are injected into the animal models (typically mice models) to form metastatic xenografts. Unfortunately, *the major flaw of* in vivo *models is the inconsistency of cells that* survive and metastasize. Furthermore, the correlation between clinical trials and animal studies is complex because of the species difference and immuno-deficiency in animal models[27–30]. Therefore, there is a need for effective 3D in vitro models that accurately mimic the natural tumor microenvironment and are relevant to human physiology. These 3D in vitro models are extremely useful in drug development by getting precise drug responses for specific targets. In the past couple of years, biomimetic *3D* in vitro models have been explored extensively, capable of imitating in vivo tissue microenvironments[31–33]. These 3D microenvironments have been shown to modify cellular adhesion, metabolic and cytokine activity, cellular morphology, and gene expression. Various 3D cancer models have recently been employed in screening different anticancer drugs[34] Another study used a 3D bioprinting approach to fabricate drug-resistant breast cancer spheroids and evaluate their response against anti-tumor agents[35]. 3D bioprinting tumor microenvironments have also been shown to help replicate primary tumor environments that may be screened for drugs[36]. A unique nano clay-based polymer–clay nanocomposite 3D in vitro bone metastatic breast cancer model[37–44] has also been demonstrated for screening of new therapeutics[45] that shows the formation of mineralized bone-tissue on nano clay-based polycaprolactone (PCL) scaffolds by vesicular delivery by osteogenically differentiated human mesenchymal stem cells (MSCs), without the need of osteogenic supplements[46–48]. Further, using osteogenically differentiated hMSCs with human breast cancer cells (commercial and patient-derived) and commercialized-prostate cancer cells, late-stage pathogenesis to bone has been reported (in static and dynamic culture conditions)[49–55] with the impact of breast cancer on osteogenesis found to be mediated by Wnt/beta-catenin signaling, at bone metastasis[56].

In the present study, for the first time, we investigated the cytotoxicity of phytochemical-enriched *R. crenulata* extracts on bone metastatic breast cancer. In addition, we report the effects of *R. crenulata* on bone health, which has yet to be explored.

Materials and methods

Materials

R. crenulata extract was purchased from One World Products, Las Vegas, NV. Human breast cancer cell lines and media: MDA-MB-231 and MCF-7 cell lines, Dulbecco's Modified Eagle Medium (DMEM) and Eagle's Minimum Essential Medium (EMEM), Fetal Bovine Serum, and Penicillin/Streptomycin were purchased from ATCC (Manassas, Virginia, USA). Polycaprolactone (PCL) (average Mn 80,000), 5-aminovaleric acid, calcium chloride (CaCl2), sodium phosphate (Na2HPO4), fish skin gelatin (FSG), TritonX-100, Tween20, and 1,4-dioxane were purchased from Sigma Aldrich (St. Louis, MO, USA). Na-MMT clay was obtained from Clay Minerals Respiratory at the University of Missouri. Human mesenchymal stem cells (hMSCs) and MSCGM bullet kit medium were purchased from Lonza (Walkersville, MD, USA). Gibco™ human recombinant insulin, Applied Biosystems™ Fast SYBR Green, Rhodamine Phalloidin, and 4′,6-diamidino-2-phenylindole (DAPI), Alamar blue cell viability reagent were purchased from Invitrogen (Waltham, MA, USA). ApoScreen® Annexin V-FITC kits were purchased from SouthernBiotech (Birmingham, AL, USA). Direct-zol RNA MiniPrep kit was purchased from Zymo Research (Irvine, CA, USA).

Preparation of PCL/in situ HAPclay 3D scaffolds

As reported earlier, freeze-drying methods were utilized to prepare PCL/in situ HAPclay scaffolds. Briefly, the procedure includes Na-MMT clay modification with 5-amino valeric acid to increase the d-spacing of the clay. Further, hydroxyapatite (HAP) was biomineralized in the intercalated nano-clay galleries, generating in situ HAP clay. Lastly, the PCL and 10% in situ HAPclay were dissolved in 1,4-dioxane, and employing the freeze-drying method, PCL/ in situ HAP clay scaffolds were prepared. The dimensions of the scaffolds used for experiments were 12 mm in diameter and 3 mm in thickness. For cell culture experiments, scaffolds were sterilized under ultraviolet light for 45 min, followed by immersion in 70% ethanol for 24 h. Next, scaffolds were washed in PBS twice, placed in 24-well plates containing culture medium, and stored in a humidified 5% CO_2 incubator at 37 °C. Incubation time was 12 h before cells were seeded.

Preparation of Rhodiola crenulata solution

A 1000 ppm stock solution of *R. crenulata* was prepared by dissolving 0.01 g of *R. crenulata* in 100 mL of 10% ethanol. This targeted phenolic phytochemicals-rich therapeutic solution was passed through a 0.22 µm filter for sterilization. The stock solution was further diluted in serial dilutions using serum-free DMEM media (ATCC). The controlled treatment defined DMEM with 8% ethanol.

Cell culture and cell seeding

MDA-MB 231 (MM 231) cells were cultured in 90% DMEM, 10% FBS, and 1% Penicillin–Streptomycin (P/S). MCF-7 cells were grown in 90% Eagle's Minimum Essential Medium (EMEM), 10% FBS, 0.01 mg/mL human recombinant insulin, and 1% P/S. Cell line passages used in experiments were between 5 to 10. In addition, cells were not utilized directly from cryopreservation. All cell cultures were maintained at 37 °C and 5% CO_2 in a humidified incubator. For 2D cultures, 1×10^5 breast cancer cells (MM 231/MCF-7) were cultured on tissue culture polystyrene (TCPS) for 10 days (cells grown for 8 days, serum-free on day 9, and treated on day 10).

The sequential cell culture method was employed for 3D Bone-metastatic (BM) cultures. First, scaffolds immersed in hMSC media were seeded with 1×10^5 MSCs (per scaffold) and kept for four hours for cell adherence. Next, media was added, and cells were cultured for 23 days to obtain bone-like extracellular matrix (ECM) formation. Cell-seeding steps have been illustrated in Fig. 1A. After 23 days, 1×10^5 human breast cancer cells (MM 231/MCF-7) were seeded on the bone-ECM scaffolds and cultured for 10 days in breast cancer media. Before seeding breast cancer cells, hMSC/bone cells were cell cycle arrested using mitomycin C at 10 µg/mL.

Cell viability assay

2D cultures of breast cancer cells (at day 10) and 3D cultures of breast cancer cells on bone ECM were serum-starved for 24 h and treated with different *Rhodiola crenulata* concentrations (0,100, 200, 400, 800 PPM) for 24 h. Cell viability of treated and untreated (control) samples was determined using Alamar blue cell viability reagent, using the manufacturer's protocol. Half maximal inhibitory concentration (IC50) values for 2D and 3D-BM cultures were calculated using nonlinear regression analysis with Graph Pad Prism (v7.04). Raw fluorescence data is included in supplementary documentation, Fig. S3.

Live/dead assay

Live/dead assay was performed on 33-day 3D bone cultures, untreated and treated with 800 ppm concentration with *R. crenulata* (*Rhodiola crenulata*). According to the manufacturer's protocol, cells were stained with a live/dead™ Cell Imaging Kit (Thermofisher Scientific, Germany). Live/dead solution was prepared by mixing the Calcein AM solution and BOBO-3 iodide. Samples were washed with PBS twice. Next, treated and untreated 3D BM samples were introduced with both live stain (Calcein AM) and dead stain (BOBO-3 iodide)). Before imaging, samples were incubated for 15 min at room temperature. Samples were imaged using a JPK Nanowizard Bio-AFM confocal system with a 10 × objective lens and FITC and TRITC wavelengths.

Flow cytometric analysis of apoptosis

After treating 2D cultures of breast cancer cells and 3D-BM breast cancer cells for 12 h with their respective IC50 concentrations, cells were harvested and washed in cold PBS 3X times. Further, the cells were resuspended in a cold Annexin Binding Buffer to a concentration of 1×10^6 cells/mL, then labeled with Propidium Iodide (P.I.) and Fluorescein isothiocyanate (FITC)- conjugated Annexin V and analyzed using BD Accuri C6 Flow cytometer and FlowJo software.

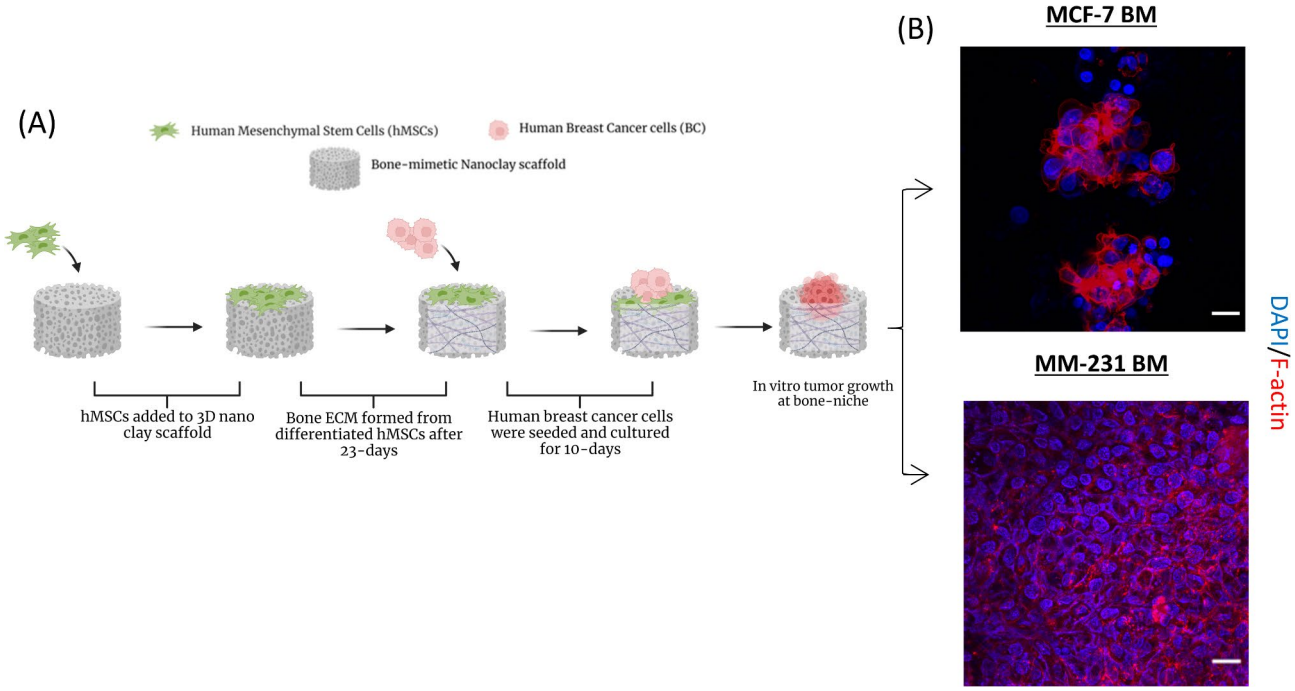

Fig. 1. (**A**) Schematic showing steps of sequential culture of human mesenchymal stem cells (hMSCs) and breast cancer cells (MM 231 and MCF-7) (**B**) The tumor morphology of 3D-BM cultures was determined by immunofluorescence staining the actin cytoskeleton with rhodamine-phalloidin and nuclei with DAPI. Mesenchymal stem cells were cultured on the testbed for 23 days. Breast cancer cells were cultured for 10 days. Scale bars, 20 µm.

Gene expression studies

Prior to the cancer cells seeding step, hMSCs were cell cycle-arrested with 10 µg/mL of Mitomycin B. Cancer cells were grown for 10 days in both 2D and 3D-BM cultures and treated with IC50 drug concentration. After 24 h of treatment, total RNA was isolated from cell-seeded scaffolds and 2D cultures using the Direct-zol RNA MiniPrep kit. Isolated RNA was reverse transcribed to synthesize cDNA using M-MLV reverse transcriptase (Promega), random primers, and thermal cycler (Applied Biosystems). Finally, Real-Time Polymerase Chain Reaction (RT-PCR) was performed using a thermal profile with a holding stage (2 min at 50 °C, 10 min at 95 °C) and a cycling stage (40 cycles of 15 s at 95 °C, and 1 min at 60 °C) on 7500 Fast Real-Time System (Applied Biosystems). The mRNA expression of p53, Bcl-2, caspase-3, and caspase-9 were evaluated. All the mRNA expressions were normalized to the housekeeping gene β-actin. Target gene expressions were calculated using the comparative C_t method ($2^{-\Delta\Delta Ct}$). The primer sequence is provided in Table S1. Raw data is included in supplementary file, Fig. S4.

Immunofluorescence staining

3D bone-metastatic cultures were fixed in 4% paraformaldehyde in PBS for 45 min, permeabilized with 0.2% TritonX-100 in PBS for 5 min, and blocked with 0.2% blocking buffer (0.2% FSG in PBS containing 0.02% Tween20) for 45 min. The actin cytoskeleton and nuclei of cells were stained with Rhodamine Phalloidin (Abcam ab235138) and DAPI (ThermoFisher Scientific 62,247), respectively. The dilution factor for rhodamine phalloidin was 1:1000. Bcl-2 and p53 antibodiesThe DAPI concentration was diluted to a working concentration of 0.1 µg/mL. The samples were observed using the JPK Nanowizard Bio-AFM confocal system. Samples were observed in a 60 × objective. Fluorescent staining of p53 and bcl-2 samples was quantified using ImageJ software.

Reactive oxygen species (ROS) assay

MM231 and MCF-7 3D bone metastatic cultures, treated and untreated, were stained following the manufacturer's protocols (Abcam, ab113851). Briefly, samples were treated with IC50 dosages of *R. crenulata* for 12 h and then washed with PBS. Next, the DCFDA solution was diluted and added to samples in the dark for 45 min at 37 °C. Lastly, all samples were rinsed with buffer before imaging. Imaging was performed using a JPK nanowizard bio-AFM confocal with a FITC filter. A 10 × objective was used to image these samples.

Mitochondrial membrane potential (MtMP) assay

Manufacturer's protocols (Cell Signaling, 13,296) were followed to perform live cell imaging. MM231 and MCF-7 3D bone metastatic cultures were treated with IC50 dosages of *R. crenulata* for 12 h and then washed with PBS twice. Next, 200 nM of TMRE labeling solution was added to all live samples. Then, samples were placed in a

CO_2 incubator for 20 min. Live cell imaging was performed using a JPK nanowizard bio-AFM confocal system using the orange-red filter. Samples were imaged using a 10 × objective lens.

Statistical analysis

The data presented is calculated as mean ± standard deviation (n = 3; three technical replicates). The statistical significance or *p*-values among multiple comparisons were determined using one-way ANOVA, followed by the post hoc Tukey test. Statistical differences between untreated cultures and cultures treated with *R. crenulata* were determined to be significant utilizing an unpaired *Student's t-test*, using GraphPad Prism v7.04. and at a 95% probability level ($p < 0.05$).

Results

Breast cancer cells grown on bone-mimetic 3D testbed form *in-vivo*-like tumoroids

We investigated the morphology of human breast cancer cells on the 3D bone mimetic testbed through immunostaining via confocal imaging. We stained the actin cytoskeleton with rhodamine-phalloidin and nuclei with DAPI. The breast cancer cells grown in 3D BM culture experienced different morphologies. MM-231 formed disorganized clusters, whereas MCF-7 formed clustered-compact tumoroids (Fig. 1). Overall, the immunostaining results show that the breast cancer cells experience strong cellular growth on the 3D BM testbed (Fig. 1B).

Breast cancer cells grown on 3D bone metastatic testbed require higher drug concentrations to achieve comparable cell viability reduction compared to 2D cultures

A cell viability assay was used to evaluate the cytotoxic effects of *R. crenulata* on 2D and 3D BM cultures. Cells were treated with 100, 200, 400, and 800 ppm of *R. crenulata* (ethanolic extracts) for 24 h, and the dose-dependent cytotoxic effects were observed in MM 231 and MCF-7 cell cultures. The IC50 was calculated from the dose–response study (Fig. S1 and S2) using curve fitting. The results indicated that *R. crenulata* reduced the proliferation of BM MCF-7 and BM MM-231, with IC50 concentrations of 316.2 ppm and 524.7 ppm, respectively (Fig. 2A,B). In contrast, the proliferation of MCF-7 and MM231 cancer cells in 2D cell cultures were reduced by treating cells with IC50 drug concentrations of 100.2 ppm and 291.4 ppm, respectively (Fig. 2A,B). Overall, the data indicated that 3D BM cultured breast cancer cells required higher concentrations of *R. crenulata* than 2D cultured breast cancer cells to inhibit the growth of 50% cell population. Furthermore, MM-231 BM required higher dosages compared to MCF-7 BM.

Bone cells experienced no cytotoxic effects with the treatment of *R. crenulata*

We evaluated the cytotoxic response of *R. crenulata* on hMSCs grown on a 3D testbed for 33 days. Bone cells were treated for 24 h with the same concentrations used for breast cancer cultures. We found no reduction in cell proliferation in all concentrations (Fig. 3). Furthermore, cell proliferation increased when treated with 400 ppm and 800 ppm concentrations. Additionally, live/dead staining confirmed that bone cells were unaffected by the treatment of 800 ppm *R. crenulata* (Fig. 3B). The data suggests that higher concentrations of *R. crenulata* can promote cell proliferation in bone cells at higher concentrations.

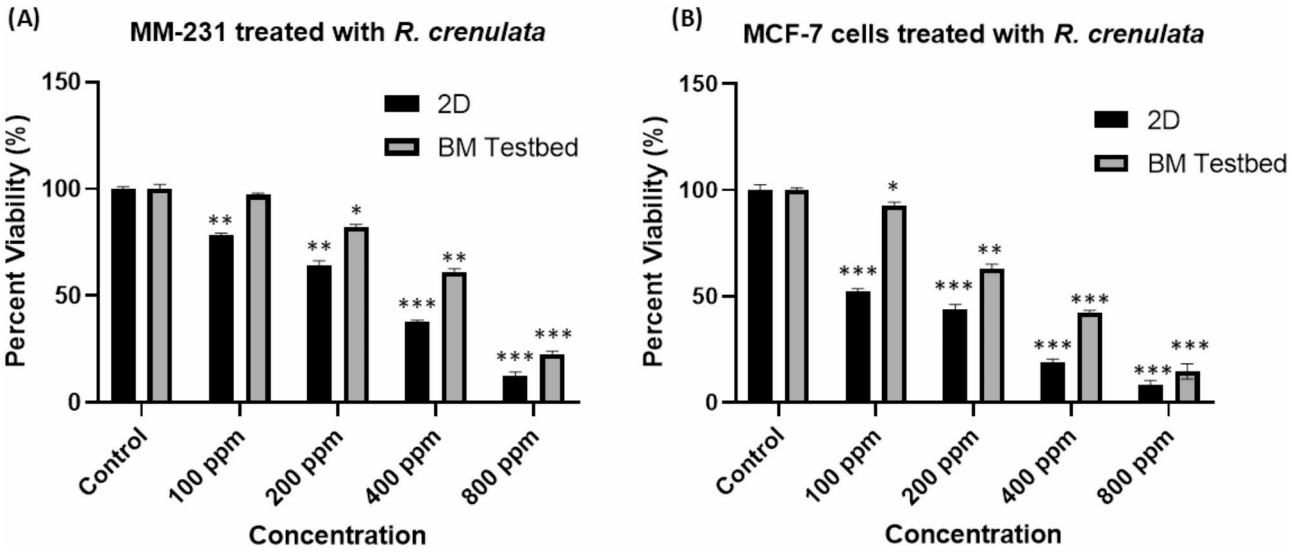

Fig. 2. The cytotoxic effects of *R. crenulata* were observed in 2D cultures of breast cancer cells (MM-231 and MCF-7) and 3D BM cultures of breast cancer cells in (**A**) MM-231 and (**B**) MCF-7 cells. The concentration dosages of 100, 200, 400, and 800 ppm of *R. crenulata* were used. Treatments were for 24 h. Alamar blue assay was used to evaluate the cell viability. The asterisk symbol (*) indicates a statistically significant difference between drug-treated and non-treated samples. $^{*}p < 0.05$ $^{**}p < 0.01$ $^{***}p < 0.001$.

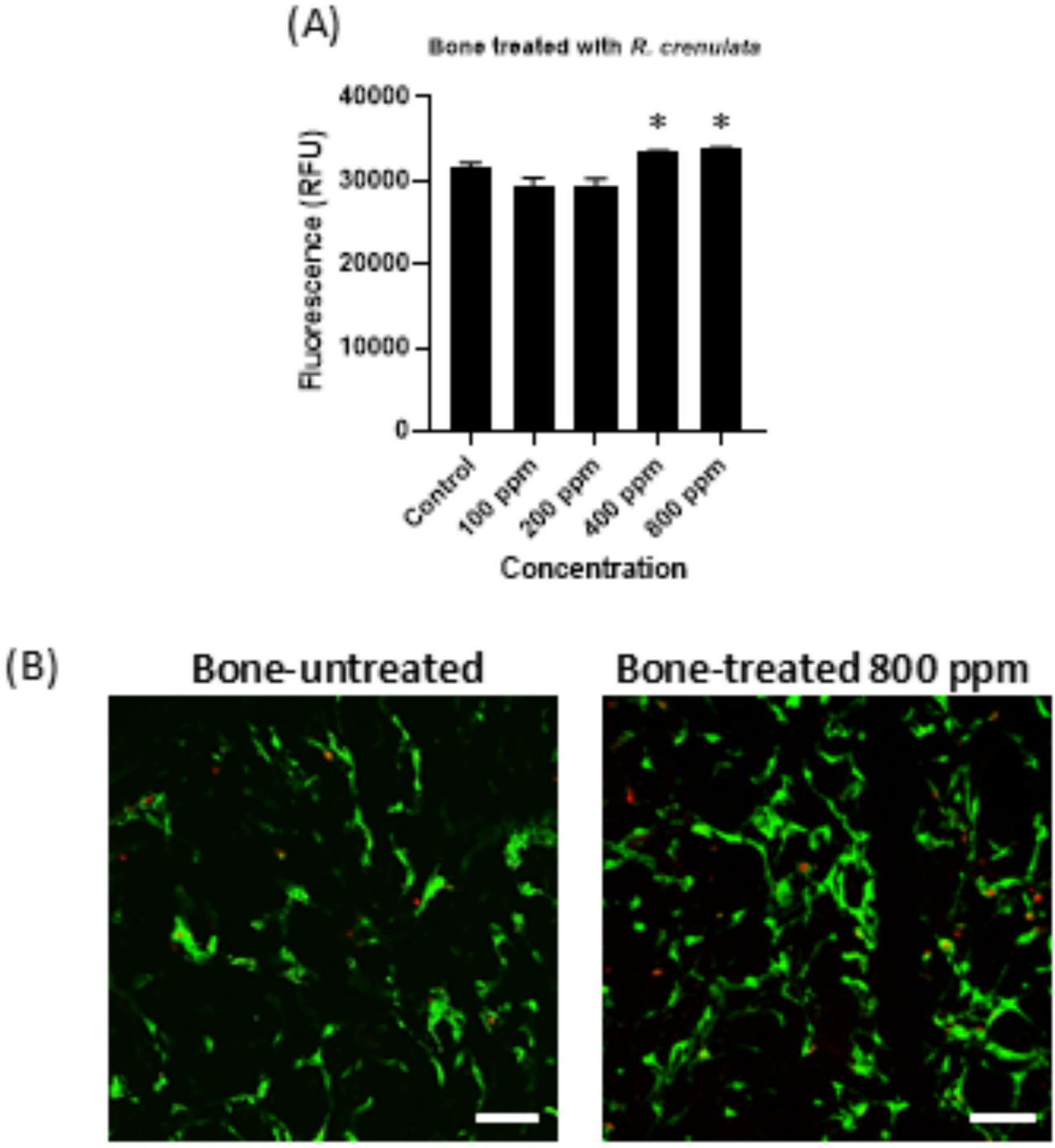

Fig. 3. The effects of *R. crenulata* on bone (33-day hMSC). (**A**) The concentration dosages used were 100, 200, 400, and 800 ppm of *R. crenulata*. Treatment was for 24 h. Alamar blue assay was used to evaluate the cell proliferation. (**B**) Live/dead imaging was performed for bone after 33 days, untreated, and treated for 24 h. The asterisk symbol (*) indicates a statistically significant difference between drug-treated and non-treated samples. Scale bar: 150 µm. $^{*}p < 0.05$ $^{**}p < 0.01$ $^{***}p < 0.001$.

R. crenulata induces apoptosis in 2D and 3D BM culture of breast cancer cells

Breast cancer cells were subjected to their respective IC50 concentrations for 12 h, followed by flow cytometric analysis using Annexin V-FITC apoptosis assay. We found that treated samples had a higher apoptosis rate than non-treated samples in 2D and 3D BM cultures. Furthermore, the data showed differences between 2 and 3D BM cultures regarding the rate of apoptosis induction (Fig. 4).

We observed a slight increase in resistance to apoptosis in 3D BM breast cancer cells compared to 2D cultures. As indicated in (Fig. 4), the apoptosis assay showed a substantial difference between control and treated

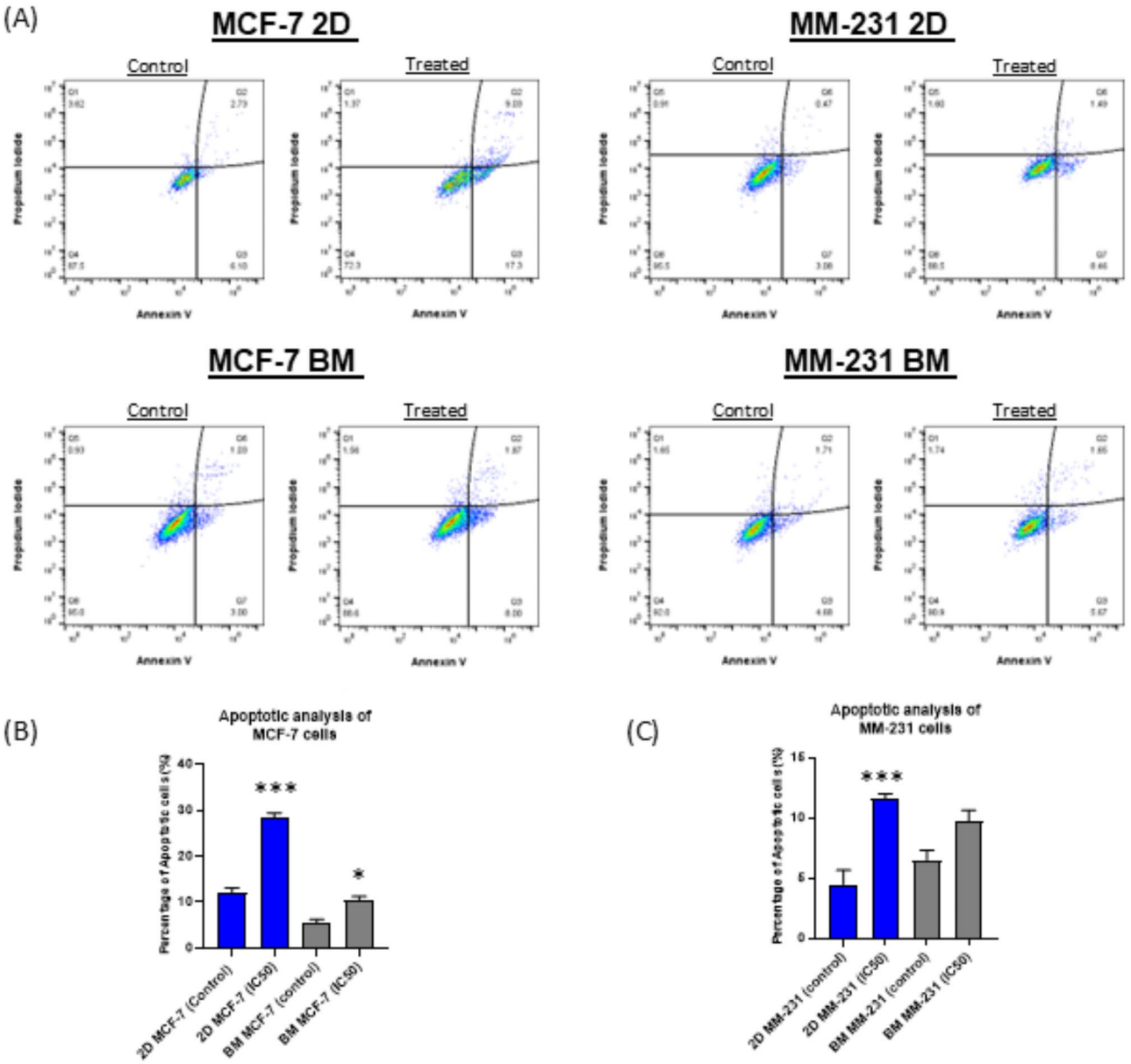

Fig. 4. (**A**) The cytotoxic effects of *R. crenulata* were observed in 2D cultures of breast cancer cells (MCF-7 and MM231) and 3D sequential culture of breast cancer cells (MCF-7 and MM231) by flow cytometric analysis. Apoptosis assay was performed on breast cancer cells after 12 h of treatment. Samples were treated with respective IC50 dosages. (**B**) Bar plots represent apoptotic cell percentages for 2D and 3D BM cultures of breast cancer cells MCF-7. (**C**) Bar plots represent apoptotic cell percentages for 2D and 3D BM breast cancer cell cultures MM 231. The asterisk symbol (*) indicates a significant difference in apoptotic percentage between drug-treated and non-treated samples in 2D and 3D cultures. $^{*}p < 0.05$ $^{**}p < 0.01$ $^{***}p < 0.001$.

samples for both 2D and 3D BM cultures. The percentage cell population of early-stage apoptosis induced by *R. crenulata* was ~ 8.46% and ~ 5.67% in 2D MM231 and 3D BM MM-231, respectively. Furthermore, the early-stage percentage of apoptosis was ~ 17.3% and ~ 8.00% in 2D MCF-7 and 3D BM MCF-7, respectively, indicating significant resistance to apoptosis in response to *R. crenulata* in 3D BM cultures versus 2D cultures.

3D bone-metastatic cultures experience increased resistance to *R. crenulata* compared to 2D cultures

In order to confirm the apoptotic activation by *R. crenulata*, we analyzed the expression of anti-apoptotic Bcl-2 and tumor suppressor p53 biomarkers in treated cultures. We specifically compared the change in mRNA expression levels between 2D cultures and 3D BM cultures after 24 h of *R. crenulata* treatment. In MCF-7 breast cancer cells, we observed that MCF-7 BM cultures experienced a ~ 2.29-fold decrease in p53 expression compared to 2D MCF-7 cultures (Fig. 5). Concomitantly, MCF-7 BM cultures experienced ~ 1.73-fold increase

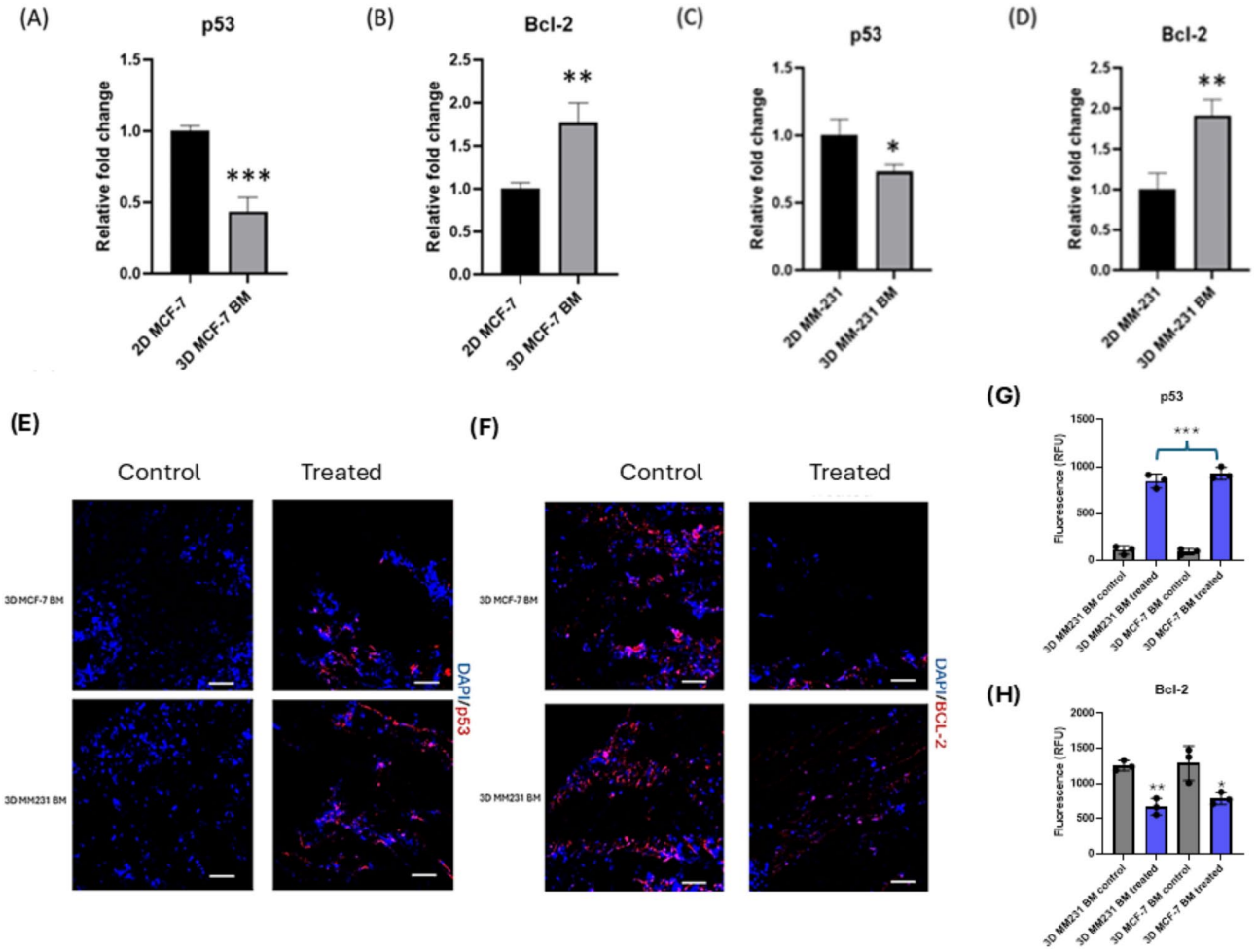

Fig. 5. Pro-and anti-apoptotic markers p53 and bcl-2 were analyzed using RT-PCR. Breast cancer samples used in these experiments were treated with IC50 dosages of *R. crenulata* for 24 h. (**A**) Analysis of p53 expression in 2D and 3D BM cultures of MCF-7breast cancer cells. (**B**) Analysis of Bcl-2 expression in 2D and 3D BM culture of MCF-7 breast cancer cells. (**C**) Analysis of p53 expression in 2D and 3D BM cultures of MM-231 breast cancer cells. (**D**) Analysis of Bcl-2 expression in 2D and 3D BM cultures of MM-231 breast cancer cells. As seen, there is a significant difference in relative expression for p53 and bcl-2 expression between 2D and Bone-metastatic (BM) treated cultures of breast cancer, indicated by $*p<0.05$, $**p<0.01$ $***p<0.001$. (**E**,**F**) Immunofluorescent images of 3D BM breast cancer cells stained with DAPI and P53/BCL-2 antibody. Images on the left are untreated samples, and images on the right are samples treated with IC50 dosages of *R. crenulata* for 24 h. Scale bar set to 150 µM. (**G**,**H**) Immunofluorescent p53 and bcl-2 staining was quantified using ImageJ NIH software. The asterisk symbol (*) indicates a significant difference between drug-treated and non-treated 3D BM cultures. $*p<0.05$ $**p<0.01$ $***p<0.001$.

in Bcl-2 expression compared to 2D MCF-7 cultures. A similar trend was observed with MM-231 BM and 2D MM-231 cultures. MM-231 BM cultures experienced ~ 1.36-fold downregulation of p53 expression compared to 2D MM-231. In addition, MM-231 BM cultures had a ~ 1.91-fold increase in bcl-2 expression compared to 2D MM-231 cultures. Overall, breast cancer cells in bone metastatic conditions experience increased resistance to apoptosis after treatment of *R. crenulata*.

To confirm p53 activation and bcl-2 inhibition on the protein level, we performed immunofluorescence imaging. In Fig. 5E, we observed an increase in p53 staining in treated BM cultures of MM231 and MCF7, compared to non-treated cultures. Alternatively, in Fig. 5F, we observed bcl-2 staining decreased in both treated cultures. Treatments of R. crenulata were IC50 dosages associated with specific samples. Figure 5G,H, confirms the observations by quantification of fluorescence.

Bone cells experience no significant changes in pro-apoptotic and anti-apoptotic markers in treated and non-treated conditions

We evaluated the apoptotic response of bone cells when treated with *R. crenulata* for 24 h and compared the relative fold change of treated and non-treated samples for bone and 3D BM culture of breast cancer cells (MM 231 and MCF-7). We analyzed the Bcl-2 expression between bone and 3D culture of breast cancer cells. In

healthy bone, we observed no significant change in treated versus non-treated samples (Fig. 6A). Further, we observed significant upregulation of p53 expression in treated samples on 3D BM culture of breast cancer cells. However, no significant change in treated versus non-treated bone cells was observed (Fig. 6B). A schematic representation of the intrinsic apoptosis pathway being activated and the role of caspase-9 in activating apoptosis is shown in Fig. 6C.

R. crenulata treatment activates Caspase-9 and decreases MtMP activity in bone metastatic breast cancer

Consecutively, we confirmed the initiation of apoptosis by evaluating the expression of caspase-9. Our results demonstrate that when 3D BM cultures were treated with *R. crenulata,* caspase-9 expression levels were upregulated significantly in treated samples compared to non-treated samples (Fig. 7A). Furthermore, MCF-7 cells experienced higher fold expression compared to MM-231 cells. Specifically, MCF-7 BM cells experienced nearly ~ 6 to 7 times upregulation in caspase-9 levels compared to untreated cultures. Compared to untreated cultures, the MM-231 BM cells experienced nearly a 5–6 times-fold activation in caspase-9 levels.

In addition to observing the changes in caspase levels, we performed live cell ROS and MtMP imaging of bone metastatic cultures. Samples were treated with IC50 dosages for 12 h. We observed a decrease in mitochondrial membrane potential intensity after treatment of *R. crenulata* for both MCF-7 BM and MM231 BM (Fig. 7B). Concurrently, ROS levels decreased in both bone metastatic cultures (Fig. 7C). However, treated MCF-7 BM expressed more ROS levels compared to treated MM231 BM.

Discussion

This study aimed to investigate the chemoresistance of bone metastasized breast cancer when treated with phenolic phytochemically rich extracts of *R. crenulata.* Breast cancer cells experience altered growth and resistance when colonizing within the bone marrow. Bone-like ECM formation is observed from osteogenically differentiated MSCs on nano clay scaffolds with enhanced migration of cancer cells in the presence of bone microenvironment[37,38,41,56]. Given the cytotoxic characteristics of *R. crenulata* towards breast cancer cells[15,17] and the efficacy of the nano clay testbed in screening anticancer drugs[57], in the present study, we studied the effect of *R. crenulata* extracts on bone metastasized breast cancer and bone cells. To assess the potential of *R. crenulata* as a treatment for advanced-stage breast cancer, we first measured the IC50 values of breast cancer cells (MM-231 and MCF-7) cultured on 2D TCPS and a 3D bone metastatic model following 24 h of *R. crenulata* treatment Previous studies have shown that R. crenulata treatment effectively inhibited the proliferation of MM-231 breast cancer cells in 2D cultures and reduced the invasion of MCF-7 cells in tumorsphere models[17,58]. Here, we observed an overall increase in cell viability in cancer cells grown on 3D bone metastatic testbed, compared to 2D cultures. Additionally, we found that MM-231 breast cancer cells were more resistant to R. crenulata than MCF-7 breast cancer cells. The calculated IC50 values were higher with MM-231 cells than with MCF-7 cells.

Alternatively, bone cells were treated with *R. crenulata* for 24 h. No studies have been reported on the cytotoxicity of *R. crenulata* on bone cells. We observed a slight increase in cell proliferation in higher concentrations, indicating the non-toxic characteristic of *R. crenulata*. To investigate the non-toxicity of the treatment further, we observed the gene expression levels of pro-apoptotic and anti-apoptotic, p53, and Bcl-2. We found no significant change in treated and non-treated bone cells. This further indicates that *R. crenulata* does not affect healthy bone cells.

There is a scarcity of non-toxic anticancer therapies available, and currently, there is no cure for bone metastasis of breast or prostate cancer. The IC50 results presented here suggest that *R. crenulata* is suitable for targeting both hormonal-positive breast cancer as well as triple-negative breast cancer at the bone metastasis site, with increased potency against hormonal-positive breast cancer. Next, we explored the ability of *R. crenulata* to induce apoptosis in 2D and 3D BM cultures. We found that treated samples had a higher apoptosis rate than non-treated samples. Furthermore, MCF-7 cells had a higher percentage of cells in the early apoptotic stage than MM231 cells in both 2D and 3D cultures.

Based on these results, we performed gene expression experiments to evaluate pro- and anti-apoptotic markers. The tumor suppressor protein, p53, is mainly involved in cell cycle regulation and DNA repair. In response to DNA damage, apoptosis can be triggered by activation of p53. Bcl-2 is part of the anti-apoptotic family of proteins, which are known to be upregulated in chemo-resistant cancer cells[59]. Activation of Bcl-2 proteins leads to inhibition or prevention of cellular apoptosis. A previous study reported that MCF-7 cells experienced a decrease in E.R. transcriptional activity, β-catenin levels, and tumorsphere formation[17]. However, no studies to date have explored *R. crenulata*-induced apoptosis in bone metastatic breast cancer. We observed activation of p53 in all treated samples. Furthermore, 2D cultures experienced higher fold expression compared to 3D BM cultures. The dysregulation of p53 can be linked to chemoresistance in cancer. Additionally, we found breast cancer cells grown in 3D bone metastatic testbed had higher fold expression of Bcl-2 compared to 2D cultures. Overall, the sequential culture of MSCs with breast cancer cells increased resistance to apoptosis.

Further, we confirmed the initiation of apoptosis by evaluating caspase-9 expression. When apoptosis occurs, cells undergo mitochondrial remodeling and increased ROS production[60]. The stimulation of caspase-9 and effector caspase signifies intrinsic apoptosis. They directly affect the mitochondria, thus regulating/initiating ROS production. Specifically, caspase-9 prevents cytochrome C from accessing complex III in the mitochondria, which allows ROS to be initially over-produced before being diminished. Our results demonstrate that when 3D cultures were treated with *R. crenulata,* the caspase-9 mRNA expression levels were upregulated. Concurrently, we observed the loss of mitochondrial membrane potential and ROS staining after treatment. At the bone site, cell death occurs, and breast cancer cells experience loss of mitochondrial health, leading to diminished ROS levels. Overall, our results suggest that phytochemically enriched *R. crenulata* extract can initiate cell death in both primary-site and secondary-site bone metastatic breast cancer.

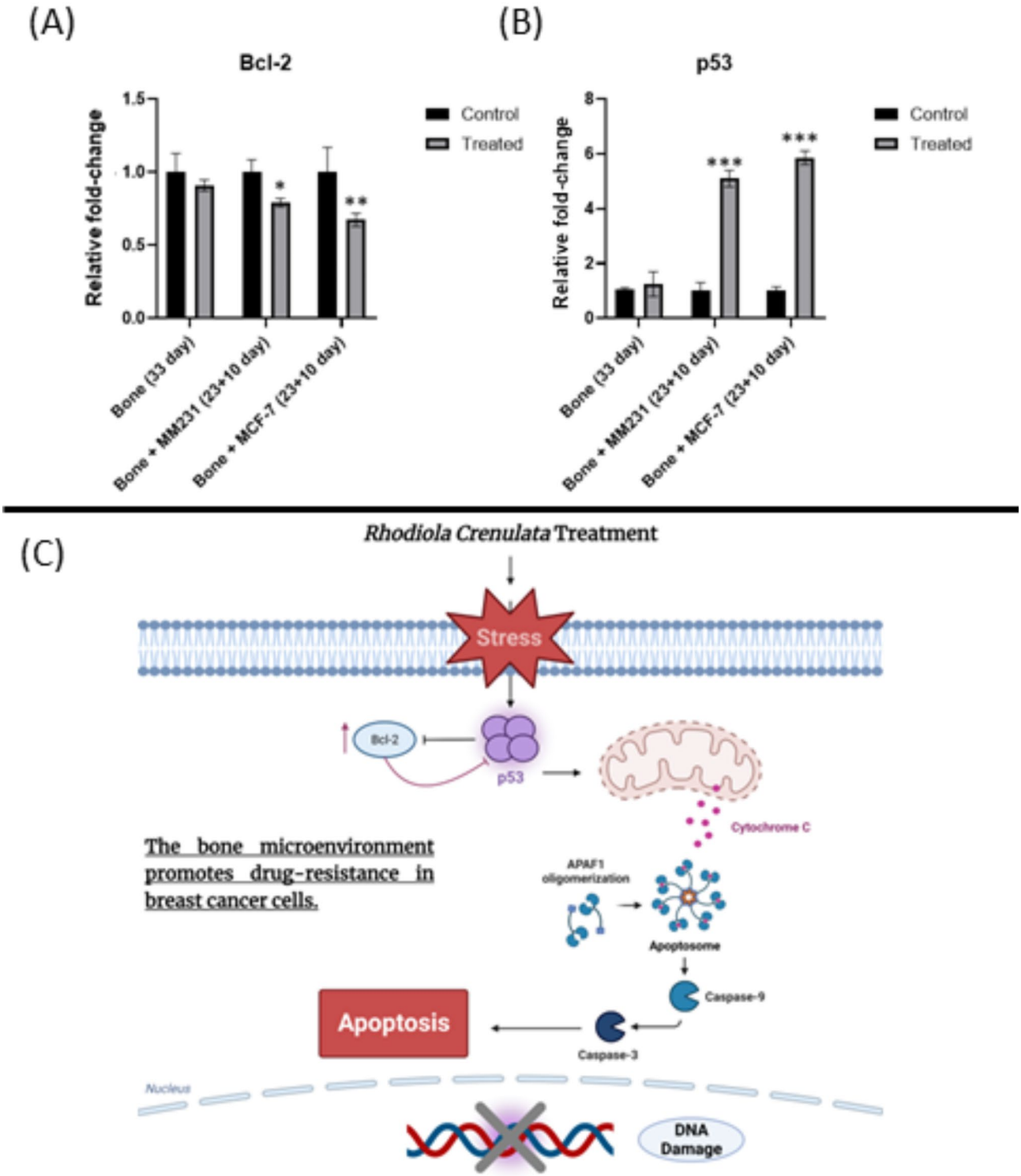

Fig. 6. Apoptotic biomarkers experienced no significant changes when the healthy bone was treated with *R. crenulata*. RT-PCR experiments were performed with samples treated with *R. crenulata* for 24 h. Samples were treated with 800 ppm *of R. crenulata*. (**A**) Gene expression of bcl-2 is represented by 33-day hMSCs (bone) compared to the 3D culture of breast cancer cells (MM 231 and MCF-7). (**B**) Gene expression of p53 is represented by 33-day hMSCs (bone) compared to 3D BM culture of breast cancer cells (MM 231 and MCF-7). Significance (*) indicates the significance of relative expression between treated and non-treated cultures. $^{*}p < 0.05$, $^{**}p < 0.01$ $^{***}p < 0.001$. Samples were processed with GraphPad Prism software. (**C**) A schematic representation of the intrinsic apoptosis pathway being activated. Specifically, the role of caspase-9 in activating apoptosis.

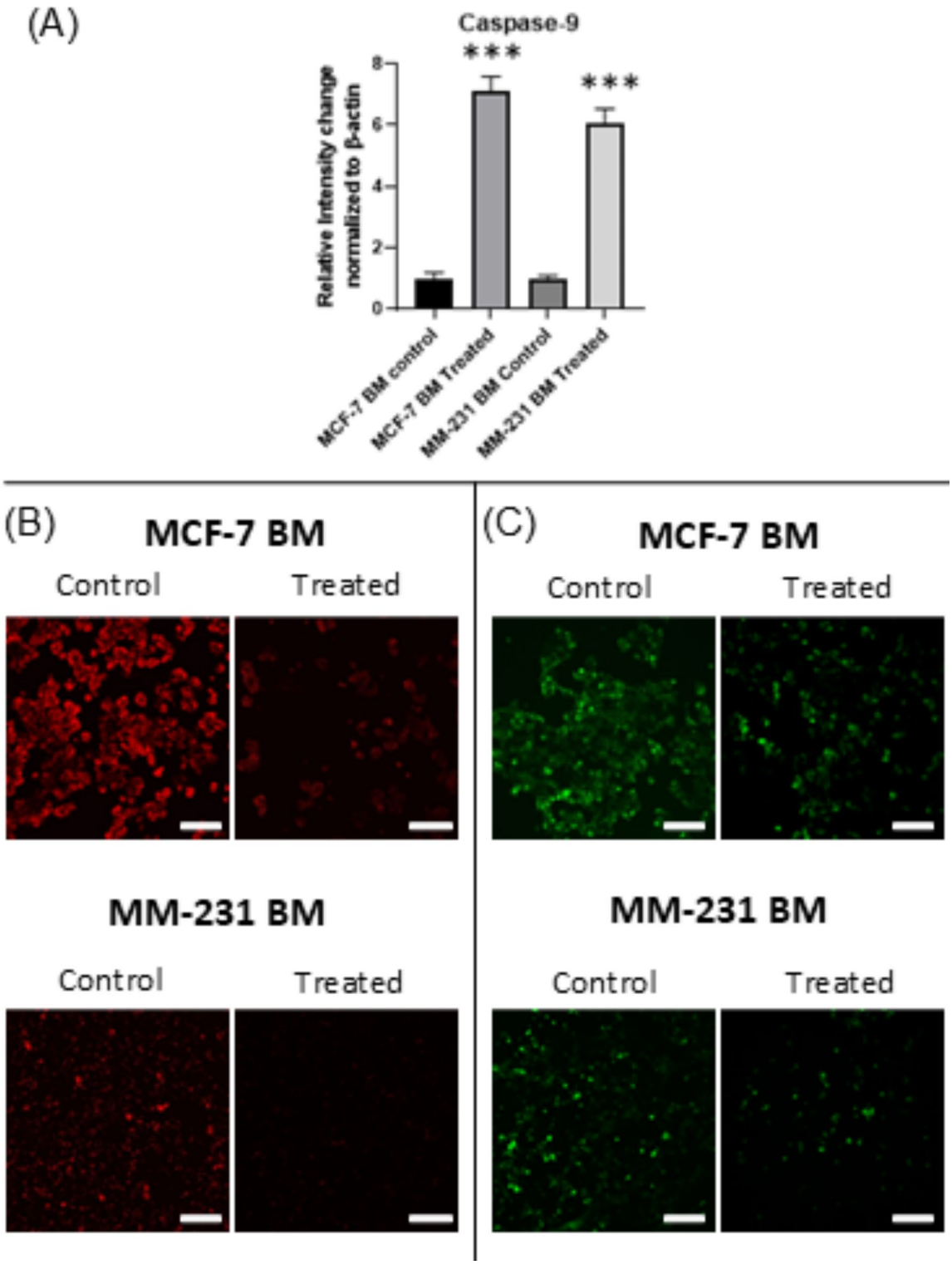

Fig. 7. *R. crenulata* activates caspase-9 in bone metastatic breast cancer (MM 231 and MCF-7). (**A**) Caspase-9 expression was measured after 24 h of treatment of *R. crenulata*. To indicate the significant difference in expression of caspase-9 between non-treated cultures and treated cultures of breast cancer cells (MM 231 & MCF-7), $^{*}p < 0.05$, $^{**}p < 0.01$ $^{***}p < 0.001$. (**B**,**C**) Live cell imaging of BM MM231 and BM MCF-7). ROS assay (green staining) and MtMP assay (red staining) were performed for treated and control samples. Samples were treated for 12 h of R. crenulata. To indicate the significant difference in expression of caspase-9 between non-treated cultures and treated cultures of breast cancer cells (MM 231 & MCF-7), $^{*}p < 0.05$, $^{**}p < 0.01$ $^{***}p < 0.001$.

To this date, *R. crenulata's* effect on bone metastasis and bone health has yet to be investigated. In the present study, we report the cytotoxic effects of *R. crenulata* on breast cancer bone metastasis. Considering all the results, we have demonstrated the in vitro efficacy of *R. crenulata* as a potential treatment for late-stage bone metastatic breast cancer. Furthermore, the cytotoxicity induced is redox-regulated. In addition, *R. crenulata* extracts are a non-toxic treatment for healthy bone cells. In future studies, we plan to investigate the redox and enzymatic activity of BM breast cancer cells before and after treatment. Overall, the 3D nano-clay bone metastatic breast cancer testbed is a promising screening tool for new therapeutics for breast cancer bone metastasis.

Conclusions

In this study, we identified R. *crenulata* as a therapeutic option for bone metastasis. We further demonstrated our 3D in vitro bone-metastatic testbed's screening ability to represent the bone metastatic niche accurately. Using the testbed, we elucidated the cytotoxic effects of R. *crenulata* against breast cancer bone metastasis and healthy bone. Considering all the results, we have demonstrated the in vitro efficacy of R. *crenulata* as a potential treatment for late-stage bone metastatic breast cancer. R. *crenulata* was able to activate caspase-9 levels and initiate apoptosis. The initiation of apoptosis was activated intrinsically and redox-regulated through the downregulation of ROS/MtMP activity. In addition to being an anticancer agent at the bone metastasis site, R. *crenulata* displayed non-toxic effects for healthy bone cells within a 24-h period. This result potentially identifies *R. crenulata* as a therapy with limiting adverse side effects, which is ideal for patient treatment. Overall, the 3D nanoclay bone metastatic breast cancer testbed is a promising screening tool for new therapeutics for breast cancer bone metastasis. Moreover, these studies demonstrate the potential of R. *crenulata* as a robust anticancer therapeutic agent that should be investigated further for its anticancer properties and non-toxic effects.

Data availability

All data generated or analyzed during this study are included in the manuscript and the accompanying supplementary document.

Received: 11 June 2024; Accepted: 5 March 2025
Published online: 18 March 2025

References

1. Siegel, R. L., Miller, K. D., Fuchs, H. E. & Jemal, A. Cancer statistics, 2022. *CA Cancer J. Clin.* **72**, 7–33, https://doi.org/10.3322/caac.21708 (2022).
2. Siegel, R. L., Giaquinto, A. N. & Jemal, A. Cancer statistics, 2024. *CA Cancer J. Clin.* **74**, 12–49, https://doi.org/10.3322/caac.21820 (2024).
3. Dillard, C. J. & German, J. B. Phytochemicals: Nutraceuticals and human health. *J. Sci. Food Agric.* **80**, 1744–1756. https://doi.org/10.1002/1097-0010(20000915)80:12%3c1744::aid-jsfa725%3e3.0.co;2-w (2000).
4. Kapinova, A. et al. Dietary phytochemicals in breast cancer research: anticancer effects and potential utility for effective chemoprevention. *Environ. Health Prev. Med.* **23**, 18. https://doi.org/10.1186/s12199-018-0724-1 (2018).
5. McEligot, A. J., Yang, S. & Meyskens, J. F. L. Redox regulation by intrinsic species and extrinsic nutrients in normal and cancer cells. *Annu. Rev. Nutr.* **25**, 261–295. https://doi.org/10.1146/annurev.nutr.25.050304.092633 (2005).
6. Ishikawa, K. et al. ROS-generating mitochondrial DNA mutations can regulate tumor cell metastasis. *Science* **320**, 661–664. https://doi.org/10.1126/science.1156906 (2008).
7. Valencia, A. & Morán, J. Reactive oxygen species induce different cell death mechanisms in cultured neurons. *Free Rad. Biol. Med.* **36**, 1112–1125. https://doi.org/10.1016/j.freeradbiomed.2004.02.013 (2004).
8. Hientz, K., Mohr, A., Bhakta-Guha, D. & Efferth, T. The role of p53 in cancer drug resistance and targeted chemotherapy. *Oncotarget* **8**, 8921–8946 (2017).
9. Todt, F. et al. Differential retrotranslocation of mitochondrial Bax and Bak. *EMBO J.* **34**, 67–80. https://doi.org/10.15252/embj.201488806 (2015).
10. Harvey, N. L. & Kumar, S. The role of caspases in apoptosis.
11. Lee, S.-Y. et al. Rhodiola crenulata extract suppresses hepatic gluconeogenesis via activation of the AMPK pathway. *Phytomedicine* **22**, 477–486. https://doi.org/10.1016/j.phymed.2015.01.016 (2015).
12. Lee, S.-Y. et al. Rhodiola crenulata and its bioactive components, salidroside and tyrosol, reverse the hypoxia-induced reduction of plasma-membrane-associated Na, K-ATPase expression via inhibition of ROS-AMPK-PKC ξ pathway. *Evid. Based Complement. Altern. Med. eCAM* **284150–284150**, 2013. https://doi.org/10.1155/2013/284150 (2013).
13. Panossian, A., Seo, E.-J. & Efferth, T. Effects of anti-inflammatory and adaptogenic herbal extracts on gene expression of eicosanoids signaling pathways in isolated brain cells. *Phytomedicine* **60**, 152881. https://doi.org/10.1016/j.phymed.2019.152881 (2019).
14. Khanna, K., Mishra, K. P., Ganju, L. & Singh, S. B. Golden root: A wholesome treat of immunity. *Biomed. Pharmacother.* **87**, 496–502. https://doi.org/10.1016/j.biopha.2016.12.132 (2017).
15. Tu, Y., Roberts, L., Shetty, K. & Schneider, S. S. *Rhodiola crenulata* induces death and inhibits growth of breast cancer cell lines. *J. Med. Food* **11**, 413–423. https://doi.org/10.1089/jmf.2007.0736 (2008).
16. Yang, Y.-N., Zhang, F., Feng, Z.-M., Jiang, J.-S. & Zhang, P.-C. Two new compounds from the roots of Rhodiola crenulata. *Journal of Asian Natural Products Research* **14**, 862–866. https://doi.org/10.1080/10286020.2012.701208 (2012).
17. Bassa, L. M. et al. Rhodiola crenulata induces an early estrogenic response and reduces proliferation and tumorsphere formation over time in MCF7 breast cancer cells. *Phytomedicine* **23**, 87–94. https://doi.org/10.1016/j.phymed.2015.11.014 (2016).
18. Mora, M. C. et al. Rhodiola crenulata inhibits Wnt/β-catenin signaling in glioblastoma. *J. Surg. Res.* **197**, 247–255. https://doi.org/10.1016/j.jss.2015.02.074 (2015).
19. Dudek, M. C. et al. Antineoplastic effects of Rhodiola crenulata treatment on B16–F10 melanoma. *Tumor Biol.* **36**, 9795–9805. https://doi.org/10.1007/s13277-015-3742-2 (2015).
20. Gauger, K., Rodriguez-Cortes, A., Hartwich, M. & Schneider, S. Rhodiola Crenulata inhibits the tumorigenic properties of invasive mammary epithelial cells with stem cell characteristics. *J. Med. Plants Res.* **4**, 446–454 (2010).
21. Wong, K. E. et al. Evaluation of Rhodiola crenulata on growth and metabolism of NB-1691, an MYCN-amplified neuroblastoma cell line. *Tumor Biol.* **40**, 1010428318779515. https://doi.org/10.1177/1010428318779515 (2018).
22. Hou, Y. et al. Rhodiola Crenulata ameliorates exhaustive exercise-induced fatigue in mice by suppressing mitophagy in skeletal muscle. *Exp. Ther. Med.* **20**, 3161–3173. https://doi.org/10.3892/etm.2020.9072 (2020).

23. Wang, X. et al. Rhodiola crenulata attenuates apoptosis and mitochondrial energy metabolism disorder in rats with hypobaric hypoxia-induced brain injury by regulating the HIF-1α/microRNA 210/ISCU1/2(COX10) signaling pathway. *J. Ethnopharmacol.* **241**, 111801. https://doi.org/10.1016/j.jep.2019.03.028 (2019).
24. Xie, N. et al. Rhodiola crenulate alleviates hypobaric hypoxia-induced brain injury via adjusting NF-κB/NLRP3-mediated inflammation. *Phytomedicine* **103**, 154240. https://doi.org/10.1016/j.phymed.2022.154240 (2022).
25. Zhang, X. et al. Neuroprotective effects of a Rhodiola crenulata extract on amyloid-β peptides (Aβ1-42)-induced cognitive deficits in rat models of Alzheimer's disease. *Phytomedicine* **57**, 331–338. https://doi.org/10.1016/j.phymed.2018.12.042 (2019).
26. Cukierman, E., Pankov, R. & Yamada, K. M. Cell interactions with three-dimensional matrices. *Curr. Opin. Cell Biol.* **14**, 633–640. https://doi.org/10.1016/s0955-0674(02)00364-2 (2002).
27. Fidler, I. J. The pathogenesis of cancer metastasis: The "seed and soil" hypothesis revisited. *Nat. Rev. Cancer* **3**, 453–458. https://doi.org/10.1038/nrc1098 (2003).
28. van der Worp, H. B. et al. Can animal models of disease reliably inform human studies?. *PLoS Med.* **7**, e1000245. https://doi.org/10.1371/journal.pmed.1000245 (2010).
29. Francia, G., Cruz-Munoz, W., Man, S., Xu, P. & Kerbel, R. S. Mouse models of advanced spontaneous metastasis for experimental therapeutics. *Nat. Rev. Cancer* **11**, 135–141. https://doi.org/10.1038/nrc3001 (2011).
30. Liu, Y. et al. Patient-derived xenograft models in cancer therapy: technologies and applications. *Signal Transduct. Target. Therapy* **8**, 160. https://doi.org/10.1038/s41392-023-01419-2 (2023).
31. Subia, B., Dey, T., Sharma, S. & Kundu, S. C. Target specific delivery of anticancer drug in silk fibroin based 3D distribution model of bone-breast cancer cells. *ACS Appl. Mater. Interfaces* **7**, 2269–2279. https://doi.org/10.1021/am506094c (2015).
32. Talukdar, S. & Kundu, S. C. Engineered 3D silk-based metastasis models: Interactions between human breast adenocarcinoma, mesenchymal stem cells and osteoblast-like cells. *Adv. Funct. Mater.* **23**, 5249–5260. https://doi.org/10.1002/adfm.201300312 (2013).
33. Talukdar, S. & Kundu, S. C. A Non-Mulberry Silk Fibroin Protein Based 3D In Vitro Tumor Model for Evaluation of Anticancer Drug Activity. *Advanced Functional Materials* **22**, 4778–4788. https://doi.org/10.1002/adfm.201200375 (2012).
34. Villata, S. et al. 3D printable acrylate polydimethylsiloxane resins for cell culture and drug testing. *Biomater. Sci.* **11**, 2950–2959. https://doi.org/10.1039/D3BM00152K (2023).
35. Hong, S. & Song, J. M. 3D bioprinted drug-resistant breast cancer spheroids for quantitative in situ evaluation of drug resistance. *Acta Biomater.* **138**, 228–239. https://doi.org/10.1016/j.actbio.2021.10.031 (2022).
36. Mi, X. et al. 3D bioprinting tumor models mimic the tumor microenvironment for drug screening. *Biomater. Sci.* **11**, 3813–3827. https://doi.org/10.1039/D3BM00159H (2023).
37. Ambre, A. H., Katti, D. R. & Katti, K. S. Nanoclays mediate stem cell differentiation and mineralized ECM formation on biopolymer scaffolds. *J. Biomed. Mater. Res. Part A* **101A**, 2644–2660. https://doi.org/10.1002/jbm.a.34561 (2013).
38. Ambre, A. H., Katti, D. R. & Katti, K. S. Biomineralized hydroxyapatite nanoclay composite scaffolds with polycaprolactone for stem cell-based bone tissue engineering. *J. Biomed. Mater. Res. Part A* **103**, 2077–2101. https://doi.org/10.1002/jbm.a.35342 (2014).
39. Katti, K. S., Ambre, A. H., Payne, S. & Katti, D. R. Vesicular delivery of crystalline calcium minerals to ECM in biomineralized nanoclay composites. *Mater. Res. Express* **2**, 045401. https://doi.org/10.1088/2053-1591/2/4/045401 (2015).
40. Katti, K. S., Ambre, A. H., Peterka, N. & Katti, D. R. Use of unnatural amino acids for design of novel organomodified clays as components of nanocomposite biomaterials. *Philos. Trans. R. Soc. A Math. Phys. Eng. Sci.* **368**, 1963–1980. https://doi.org/10.1098/rsta.2010.0008 (2010).
41. Ambre, A., Katti, K. S. & Katti, D. R. In situ mineralized hydroxyapatite on amino acid modified nanoclays as novel bone biomaterials. *Mater. Sci. Eng. C* **31**, 1017–1029. https://doi.org/10.1016/j.msec.2011.03.001 (2011).
42. Sikdar, D., Pradhan, S. M., Katti, D. R., Katti, K. S. & Mohanty, B. Altered phase model for polymer clay nanocomposites. *Langmuir* **24**, 5599–5607. https://doi.org/10.1021/la800583h (2008).
43. Kar, S., Katti, D. R. & Katti, K. S. Evaluation of quasi-static and dynamic nanomechanical properties of bone-metastatic breast cancer cells using a nanoclay cancer testbed. *Sci. Rep.* **11**, 3096–3096. https://doi.org/10.1038/s41598-021-82664-9 (2021).
44. Kar, S., Katti, D. R. & Katti, K. S. Fourier transform infrared spectroscopy based spectral biomarkers of metastasized breast cancer progression. *Spectrochim. Acta Part A Mol. Biomol. Spectrosc.* **208**, 85–96. https://doi.org/10.1016/j.saa.2018.09.052 (2019).
45. Kar, S., Katti, D. R. & Katti, K. S. Bone interface modulates drug resistance in breast cancer bone metastasis. *Colloids Surf. B Biointerfaces* **195**, 111224. https://doi.org/10.1016/j.colsurfb.2020.111224 (2020).
46. Kundu, K., Katti, D. R. & Katti, K. S. Tissue-engineered interlocking scaffold blocks for the regeneration of bone. *JOM* **72**, 1443–1457. https://doi.org/10.1007/s11837-020-04027-5 (2020).
47. Kundu, K., Afshar, A., Katti, D. R., Edirisinghe, M. & Katti, K. S. Composite nanoclay-hydroxyapatite-polymer fiber scaffolds for bone tissue engineering manufactured using pressurized gyration. *Compos. Sci. Technol.* **202**, 108598. https://doi.org/10.1016/j.compscitech.2020.108598 (2021).
48. Kundu, K., Jaswandkar, S. V., Katti, D. R. & Katti, K. S. Initial upsurge of BMPs enhances long-term osteogenesis in in-vitro bone regeneration. *Materialia* **26**, 101576. https://doi.org/10.1016/j.mtla.2022.101576 (2022).
49. Kar, S., Molla, M. D. S., Katti, D. R. & Katti, K. S. Tissue-engineered nanoclay-based 3D in vitro breast cancer model for studying breast cancer metastasis to bone. *J. Tissue Eng. Regen. Med.* **13**, 119–130. https://doi.org/10.1002/term.2773 (2019).
50. Katti, K. S. et al. Sequential culture on biomimetic nanoclay scaffolds forms three-dimensional tumoroids. *J. Biomed. Mater. Res. Part A* **104**, 1591–1602. https://doi.org/10.1002/jbm.a.35685 (2016).
51. Molla, M. D. S., Katti, D. R. & Katti, K. S. In vitro design of mesenchymal to epithelial transition of prostate cancer metastasis using 3D nanoclay bone-mimetic scaffolds. *J. Tissue Eng. Regen. Med.* **12**, 727–737. https://doi.org/10.1002/term.2492 (2017).
52. Molla, M. D. S., Katti, D. R. & Katti, K. S. An in vitro model of prostate cancer bone metastasis for highly metastatic and non-metastatic prostate cancer using nanoclay bone-mimetic scaffolds. *MRS Adv.* **4**, 1207–1213. https://doi.org/10.1557/adv.2018.682 (2019).
53. Jasuja, H. et al. Patient-derived breast cancer bone metastasis in vitro model using bone-mimetic nanoclay scaffolds. *J. Tissue Eng. Regen. Med.* **2023**, 5753666. https://doi.org/10.1155/2023/5753666 (2023).
54. Jasuja, H., Kar, S., Katti, D. R. & Katti, K. Perfusion bioreactor enabled fluid-derived shear stress conditions for novel bone metastatic prostate cancer testbed. *Biofabrication*. https://doi.org/10.1088/1758-5090/abd9d6 (2021).
55. Jasuja, H., Jaswandkar, S. V., Katti, D. R. & Katti, K. S. Interstitial fluid flow contributes to prostate cancer invasion and migration to bone; study conducted using a novel horizontal flow bioreactor. *Biofabrication* **15**, 025017. https://doi.org/10.1088/1758-5090/acc09a (2023).
56. Kar, S., Jasuja, H., Katti, D. R. & Katti, K. S. Wnt/β-catenin signaling pathway regulates osteogenesis for breast cancer bone metastasis: Experiments in an in vitro nanoclay scaffold cancer testbed. *ACS Biomater. Sci. Eng.* **6**, 2600–2611. https://doi.org/10.1021/acsbiomaterials.9b00923 (2019).
57. Kar, S., Katti, D. R. & Katti, K. S. Bone interface modulates drug resistance in breast cancer bone metastasis. *Colloids Surf. B Biointerfaces* **195**, 10. https://doi.org/10.1016/j.colsurfb.2020.111224 (2020).
58. Tu, Y., Roberts, L., Shetty, K. & Schneider, S. S. Rhodiola crenulata induces death and inhibits growth of breast cancer cell lines. *J. Med. Food* **11**, 413–423 (2008).
59. Knappskog, S. & Lønning, P. E. P53 and its molecular basis to chemoresistance in breast cancer. *Expert Opin. Ther. Targets* **16**, S23–S30. https://doi.org/10.1517/14728222.2011.640322 (2012).

60. Zorova, L. D. et al. Mitochondrial membrane potential. *Anal. Biochem.* **552**, 50–59. https://doi.org/10.1016/j.ab.2017.07.009 (2018).

Acknowledgements
This work was supported by NSF under grant OIA NDACES-1946202. Partial support from Agriculture Products Utilization Commission North Dakota Grant 20-216 and NIH (DaCCoTA) grant U54GM128729 is also acknowledged.

Author contributions
PR: Data curation; Formal analysis; Investigation; Methodology; Validation; Writing—original draft; and Writing—review & editing. HJ: Data curation; Formal analysis; Investigation; Methodology; Validation; Writing—original draft; and Writing—review & editing. DS: Data curation; Formal analysis; Investigation; Methodology; Validation; Writing—original draft; and Writing—review & editing. BVP: Data curation; Formal analysis PVP: Data curation; Formal analysis. HKG: Data curation; Formal analysis. DRK: Conceptualization; Data curation; Formal analysis; Funding acquisition; Investigation; Methodology; Project administration; Resources; Software; Supervision; Validation; Visualization; Roles/Writing—original draft; and Writing—review & editing; KS: Conceptualization; Data curation; Formal analysis; Funding acquisition; Investigation; Methodology; Project administration; Resources; Software; Supervision; Validation; Visualization; Roles/Writing—original draft; and Writing—review & editing; KSK: Conceptualization; Data curation; Formal analysis; Funding acquisition; Investigation; Methodology; Project administration; Resources; Software; Supervision; Validation; Visualization; Roles/Writing—original draft; and Writing—review & editing.

Declarations

Competing interests
The authors declare no competing interests.

Additional information
Supplementary Information The online version contains supplementary material available at https://doi.org/10.1038/s41598-025-93274-0.

Correspondence and requests for materials should be addressed to K.S.K.

Reprints and permissions information is available at www.nature.com/reprints.

Publisher's note Springer Nature remains neutral with regard to jurisdictional claims in published maps and institutional affiliations.